Langmuir

Article

pubs.acs.org/Langmuir

Consequences of Water between Two Hydrophobic Surfaces on Adhesion and Wetting

Adrian P. Defante, Tarak N. Burai, Matthew L. Becker, and Ali Dhinojwala*

Department of Polymer Science, The University of Akron, Akron, Ohio 44325, United States

Supporting Information

ABSTRACT: The contact of two hydrophobic surfaces in water is of importance in biology, catalysis, material science, and geology. A tenet of hydrophobic attraction is the release of an ordered water layer, leading to a dry contact between two hydrophobic surfaces. Although the water-free contact has been inferred from numerous experimental and theoretical studies, this has not been directly measured. Here, we use surface sensitive sum frequency generation spectroscopy to directly probe the contact interface between hydrophobic poly(dimethylsiloxane) (PDMS) and two hydrophobic surfaces (a self-assembled monolayer, OTS, and a polymer coating, PVNODC). We show that the interfacial structures for OTS and PVNODC are identical in dry contact but that they differ dramatically in wet contact. In water, the PVNODC surface partially rearranges at grain boundaries, trapping water at the contact interface leading to a 50% reduction in adhesion energy compared to OTS−PDMS contact. The Young−Dupré equation, used extensively to calculate the thermodynamic work of adhesion, predicts no differences between the adhesion energy for these two hydrophobic surfaces, indicating a failure of this well-known equation when there is a heterogeneous contact. This study exemplifies the importance of interstitial water in controlling adhesion and wetting.

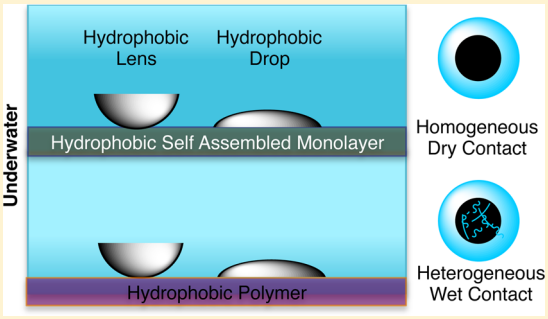

INTRODUCTION

Hydrophobic interactions are used to explain many phenomena prevalent in physical and biological sciences, such as protein folding,[1] self- assembly,[2−6] dewetting,[7] adhesion,[8] friction,[9] adsorption,[10] water transport,[11,12] and chemical reactions.[13] The hydrophobic adhesion is defined as the difference in interfacial energy between two hydrophobic surfaces before and after contact underwater.[14] Experimentally, direct force measurements[15−17] or contact angle measurements[18] have been used to measure adhesion energy where the contact between two hydrophobic surfaces is assumed to be dry. This drying phenomenon has been supported by molecular simulations between hydrophobic surfaces[6,19,20] but never experimentally verified.

Recent findings are challenging the concept of dry hydrophobic contact. X-ray crystallography has observed the presence of water within protein cavities of varying hydrophobicity which can affect the strength of protein−ligand binding.[21,22] Simulations have also shown that water can be sequestered between hydrophobic plates with a relatively small centralized hydrophilic patch.[23] Ambiguity also remains as to how dry contact is established underwater. The entropy gained by releasing interstitial water between hydrophobic surfaces prior to contact could be facilitated by a depleted density profile at the hydrophobic water interface,[24,25] the presence of nanobubbles,[26] or the concept of increased fluctuations in interfacial water.[27]

To understand the role of water in adhesion and contact angles, we have used surface sensitive sum frequency generation spectroscopy (SFG) to directly study the contact interface between two hydrophobic surfaces underwater. Octadecyltrichlorosilane monolayer (OTS) and spin-coated semicrystalline ($T_m \sim 50°$) poly(vinyl-*n*-octadecyl carbamate) films (PVNODC) were chosen because these surfaces are considered to be equally hydrophobic.[28] Both of these surfaces are composed of well-ordered all-trans long hydrophobic chains with surface terminal methyl groups, which results in high static water contact angles and low contact angle hysteresis.[29−32] When in contact with water, the surface composition of PVNODC changes to expose hydrophobic methylene groups at the crystalline grain boundaries in addition to the ordered terminal methyl groups in the crystalline regions.[31] The Johnson−Kendall−Roberts (JKR) approach was used to measure the adhesion energy between a deformable hydrophobic poly(dimethylsiloxane) (PDMS) lens in contact with OTS and PVNODC in dry and wet conditions. In dry conditions, both surfaces exhibited similar adhesion energies using the JKR approach and the Young−Dupré equation. We observed 50% lower work of adhesion for PVNODC compared to OTS surfaces from underwater JKR experiments. Surprisingly, the thermodynamic works of adhesion underwater

Received: November 24, 2014
Revised: February 8, 2015
Published: February 10, 2015

ACS Publications © 2015 American Chemical Society

DOI: 10.1021/la504564w
Langmuir 2015, 31, 2398−2406

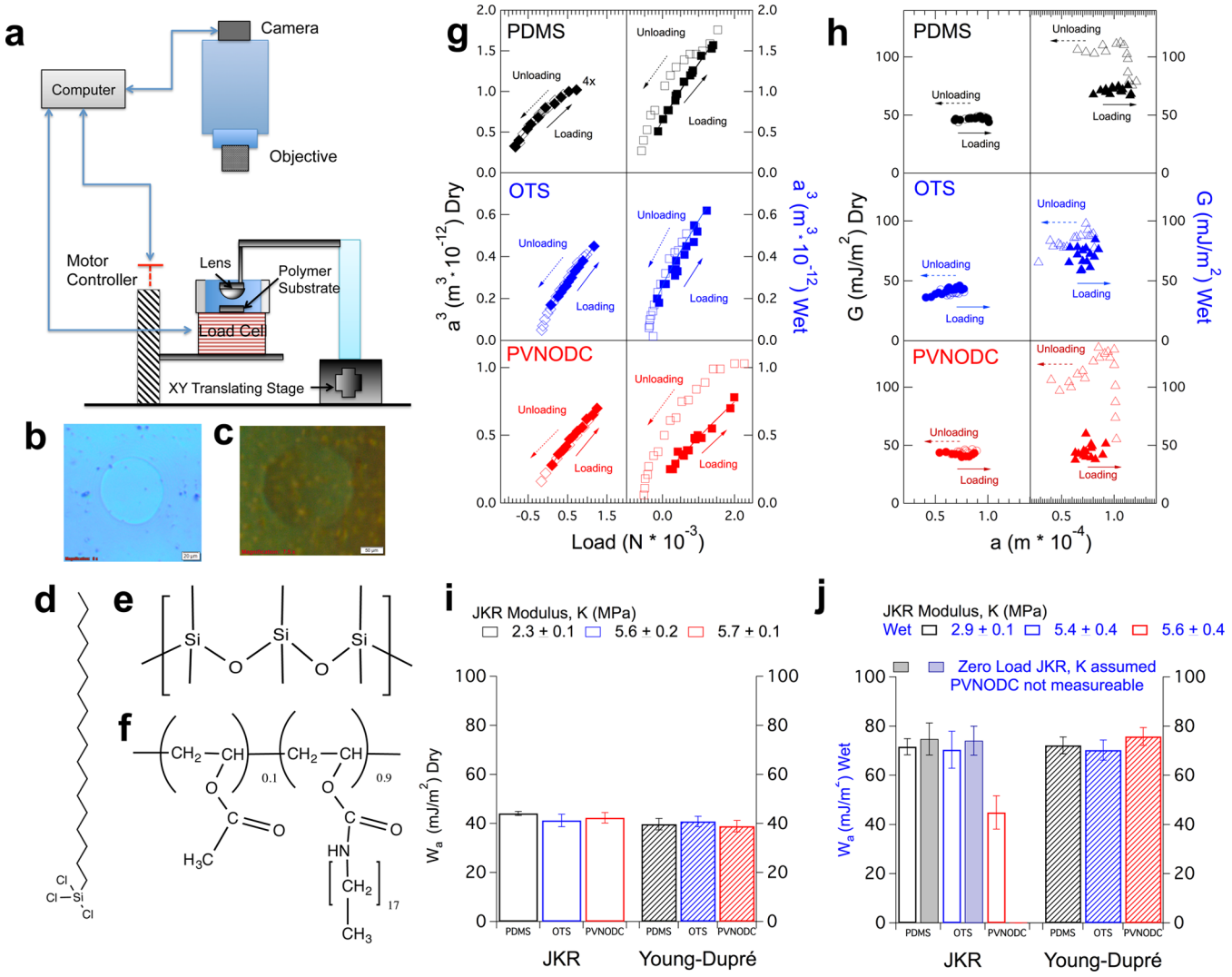

Figure 1. JKR adhesion energy plots in dry and wet conditions. (a) Schematic of JKR apparatus. Optical microscopy images for (b) dry contact (scale bar 20 μm magnification 8×) and (c) wet contact (scale bar 50 μm, magnification 7.5×). Underwater contrast was achieved with a diffraction grating placed under sample. Chemical structures for (d) OTS, (e) PDMS, and (f) PVNODC. (g) PDMS−PDMS, dry contact 4× for clarity, PDMS−OTS, and PDMS−PVNODC JKR adhesion: dry (left), wet (right). The strain energy release rate, G, is related to adhesion energy and under thermodynamic equilibrium equals the work of adhesion for nonhysteretic behavior shown for (h) PDMS−PDMS, PDMS−OTS, and PDMS−PVNODC in dry (left) conditions for all three surfaces. Hysteresis is observed for the wet (right) case for all three systems. Adhesion results measured by JKR and calculated by Young−Dupré (i) in dry conditions and (j) wet conditions. Included are JKR results measured under zero load.

calculated from the Young−Dupré equation for both PVNODC and OTS in contact with liquid were identical.

In contact mechanics, the underwater adhesion energy is dictated by the actual contact area, and a lower adhesion energy implies incomplete contact due to the presence of interstitial water.[29] This hypothesis was directly confirmed using SFG by the observation of a water layer between elastomeric PDMS−PVNODC contact. In comparison to contact mechanics, the contact angle measurements are only sensitive to the surface structure near the contact line,[33] and the contact area is assumed to be homogeneous. However, SFG measured water between the liquid PDMS−PVNODC contact interface and this indicates the breakdown of the Young−Dupré equation in predicting the thermodynamic work of adhesion (W_a) when the contact region is heterogeneous. The subtle rearrangements of the hydrophobic side chains of PVNODC in contact with water lead to lower adhesion energy and wet contact. Our results highlight the importance of understanding the role of interstitial water in understanding adhesion, a topic relevant for numerous scientific disciplines.

EXPERIMENTAL SECTION

An Olympus microscope was used to measure lens' radii, which were analyzed by CellSens software. A home-built JKR apparatus shown in Figure 1a measured the W_a in dry and wet environments. The load cell, Futek LSB 200, was attached to a translating stage moving in the Z direction with a maximum capacity of 1 N. A zigzag glass arm was fixed to an X−Y translating base. The ribbon and lens were placed on the glass support which allowed the load cell with the substrate to approach the lens.[30] Prior to all wet measurements, all glassware and metal components were thoroughly cleaned. In wet conditions, PDMS, OTS, or PVNODC was prepared on sapphire plates for optical contrast and submerged in a glass dish.

All components were placed on a vibration damping table at room temperature. A lid was designed to minimize evaporation loss, 1−3 μN/min, and was accounted for in the loading and unloading values. The rubber lens was carefully brought into contact with a computer-controlled high-resolution picometer motor. After confirming contact

DOI: 10.1021/la504564w
Langmuir 2015, 31, 2398−2406

with the microscope, the lens was loaded in 0.1−0.2 mN intervals at 0.02 μm/s every minute. Unloading measurements were done continuously at a rate of 0.01 μm/s. Loading and unloading rates were done at the slowest rate allowed by the instrumentation. The lens traveled an estimated distance of 4−6 μm in one direction as measured by a 0-15-0 dial test indicator.

To obtain an underwater loading curve, the lens was brought into contact under various preloads with the substrate and then translated using the X-Y stage until strong optical contrast was achieved. Strong contrast was indicative of good contact underwater, observed in zero load measurements. By translating the lens, equilibrium contact was established quickly. This procedure was done at various preloads to collect data for a loading curve. For unloading underwater, the lens was preloaded and translated to achieve equilibrium contact, followed by continuous unloading. Zero load measurements were achieved by gently placing a lens on top of the substrate of interest and recording the contacting image. To determine the W_a, the modulus K was assumed from the JKR loading experiments in dry and wet conditions.

A Ramehart contact angle goniometer was used to measure contact angles to determine wettability. Water contact angles, advancing and receding, were measured at a 30° tilt. Hexadecane and PDMS contact angles were taken within 5 s of drop application to avoid swelling in dry conditions. For underwater contact angles, surfaces were submerged in a quartz container. PDMS was dropped onto the surfaces underwater, and 5 min was allowed for the sample to equilibrate. No noticeable swelling was observed with liquid PDMS on PDMS cured sheets underwater.

SFG is a second-order nonlinear optical technique sensitive to the concentration and orientation of interfacial molecules. Under the electric dipole approximation, the SFG signal is generated at a surface, and the contribution from the isotropic bulk is negligible. The SFG measurement involves mixing a visible laser beam of a fixed wavelength with a tunable infrared (IR) beam. The SFG signals are enhanced when the scanning IR wavenumber overlaps with the stretching vibrations of the chemical groups at the surface. Chemical identity and orientation of molecular species at an interface can be determined by SFG with a combination of polarized input and output beams in conjunction with the location of the resonance enhanced SFG signal.[34,35] The critical angles, 42°, 16°, and 8° with respect to the surface normal of an equilateral sapphire prism, were chosen to selectively probe the polymer/air, polymer/water, and polymer/elastomer interfaces, respectively. SFG spectra were acquired at room temperature with a picosecond Spectra-Physics laser system producing a tunable wavelength IR beam (1 ps pulse width and 1 kHz repetition rate) and a visible beam (800 nm wavelength, 1 ps pulse width, and 1 kHz repetition rate). The laser beam size was estimated to be 1 mm^2 focused over a spot area of 2.3 mm^2, when the lens is in mechanical contact. The lens' radii (R) were between 2.6 and 3.0 mm with a contact radius (a) of 0.85−0.9 mm. The applicability for JKR occurs when $a/R < 0.4$. The SFG spectra were collected by scanning in ranges from 2200 to 3800 cm^{-1} in SSP and PPP polarizations (s-polarized SFG output, s-polarized visible input, and p-polarized IR input for SSP and all p-polarizations in PPP configuration). The resolution of the spectrometer is estimated to be 5 cm^{-1}. The resulting spectra were modeled for peak identification using a Lorenztian fitting function[36]

$$I(\mathrm{SFG}) \propto \left| \chi_{\mathrm{eff,NR}} + \sum \frac{A_q e^{i\phi_q}}{\omega_{\mathrm{IR}} - \omega_q - i\Gamma_q} \right|^2 \quad (1)$$

where $\chi_{\mathrm{eff,NR}}$ describes the nonresonant contribution. A_q, Γ_q, and ω_q are the amplitude, damping constant, and angular frequency of the qth vibrational resonance, respectively.

RESULTS AND DISCUSSION

Figures 1g,h show the JKR adhesion measurements for PDMS lenses in contact with PDMS, OTS, and PVNODC (Figures 1d−f) surfaces in dry and wet contact. The observed contact areas are shown in Figures 1b,c. For adhesion theory and analysis see the Supporting Information. Figures 1i,j summarize the work of adhesion (W_a) in dry contact calculated using the JKR equation (see Supporting Information, Table 1, for numerical results). We also report the W_a calculated using JKR measurements under zero load following the procedure reported by Chaudhury and co-workers.[29] The JKR measurements for dry PDMS−PDMS contact have been reported before, and they serve as a control to judge the validity of our experimental technique.[29] The results of adhesion energy and the small hysteresis between approach and retraction are consistent with those reported in the literature.[29,30,37] The JKR measurements for PDMS−OTS in dry and wet conditions are similar to those measured for PDMS−PDMS contact. The JKR results for PDMS−PVNODC are only similar to PDMS−PDMS and PDMS−OTS under dry conditions.[31,38] However, the W_a for PDMS−PVNODC in water is much lower than that for PDMS−PDMS and PDMS−OTS contact. A similar conclusion is reached using the results from zero load measurements, where some PDMS lenses floated atop the PVNODC substrate, while others adhered poorly. Additionally, the adhesion hysteresis is much larger for PDMS−PVNODC compared with PDMS−OTS and PDMS−PDMS underwater.

Figures 1i,j also summarize the W_a calculated by measuring contact angles (θ) of PDMS on all three surfaces in air (a) or underwater (w) using the Young−Dupré equation (Table 1)

$$W_a = \gamma_{\mathrm{PDMS,(a\ or\ w)}}(1 + \cos(\theta)_{\mathrm{(a\ or\ w)}}) \quad (2)$$

Table 1. Contact Angle (in deg) Measurements

substrate	static[a,d]	adv[a,d]	rec[a,d]	static[b,d]	static[c,d]	static[c,e]
PDMS	106	110	102	42	21	39
OTS	108	109	103	38	27	43
PVNODC	106	108	98	45	12	30

[a]Water. [b]Hexadecane. [c]PDMS; std ± 2°. [d]Dry. [e]Wet.

where $\gamma_{\mathrm{PDMS,(a\ or\ w)}}$ is the interfacial tension for PDMS−air (a) or PDMS−water (w) (section SI2). The results calculated from the Young−Dupré equation for liquid PDMS−PVNODC are consistent with JKR measurements for PDMS−OTS contact in all conditions and are almost 50% higher than the values measured using JKR for PDMS−PVNODC contact in water.

To understand the differences between OTS and PVNODC surfaces, we used surface sensitive SFG to probe the dry and wet contact interface (Figure 2a). Figures 2b,c show the SFG results, measured in dry conditions replicating those used in JKR experiments (before, during, and after contact). For both OTS and PVNODC the prominent peaks in the SFG spectra are for ordered terminal methyl groups,[31,36] depicted in Figure 2d, characteristic of low-energy surfaces depicted. The absence of methylene signals indicates an all-trans conformation of the hydrophobic alkyl chains. The SFG spectral features after contact are similar to the pristine surfaces before contact, confirming that there are minor surface rearrangements upon contact for both OTS and PVNODC surfaces. These results are also consistent with the small hysteresis observed in the JKR experiments under dry conditions. The SFG results of liquid PDMS in dry contact with OTS have been reported elsewhere and are identical to our results of dry elastomeric PDMS−OTS contact.[39] Given that the adhesion energies of OTS and PVNODC are similar in dry conditions for all macroscopic measurement techniques, we expect the molecular features of liquid PDMS in contact with OTS and PVNODC to be similar.

DOI: 10.1021/la504564w
Langmuir 2015, 31, 2398−2406

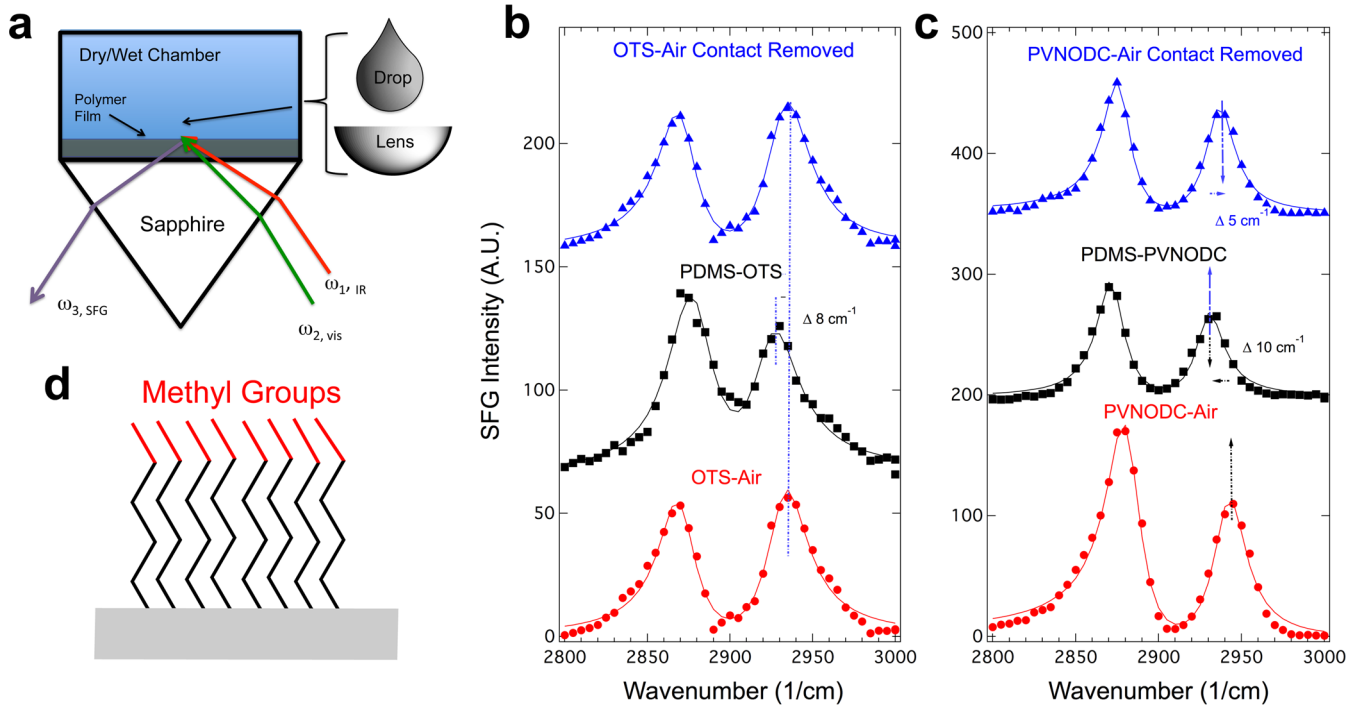

Figure 2. SFG spectroscopy of dry mechanical contact of elastomeric PDMS on OTS and PVNODC. SFG total internal reflection (TIR) geometry for a (a) contacting lens or contacting drop in dry or wet conditions. (b) SFG SSP spectra of PDMS−OTS and (c) PDMS−PVNODC before, during, and after contact. (d) Sketch of OTS or PVNODC structure at the air interface.

Figures 3a,b show the SFG measurements underwater for PDMS−OTS contact, presented in the hydrocarbon (2800−3100 cm^{-1}) and water (3100−3800 cm^{-1}) regions. As previously discussed, the OTS−air surface is covered with terminal methyl groups. Underwater, the OTS structure is relatively unchanged, with perhaps a small shoulder visible in the methylene region (2845 cm^{-1}) (Figure 3f). This small shoulder could be due to gauche defects generated at the grain boundaries. The magnitude of this methylene peak depends on the quality of the OTS monolayer, and the structure underwater is very sensitive to these defects.[40] The position of the $CH_{3,Fermi}$ peak is slightly red-shifted (Δ 7 cm^{-1}), consistent with the hypothesis that these chemical groups are in direct contact with water and that there is no depletion layer between the water and the hydrophobic OTS surface.[24]

The spectral signature in the water region for OTS−water interface shows a strong, hydrogen-bonded water peak (3100 cm^{-1})[41] (Figure 3b). In comparison, the OTS−air interface is relatively dry where a small signature in the OH region could be due to the interface between OTS and the underlying OH groups on the sapphire substrate. The contact interface between PDMS−OTS is almost identical to the dry OTS surface, except that a strong, hydrogen-bonded water peak observed near 3100 cm^{-1} is absent, indicating that the contact interface underwater is dry. Interestingly, the weak methylene peak is also diminished in intensity indicating a dry OTS−PDMS contact interface. After separating the PDMS−OTS contact, we recover the structure observed for OTS in contact with water. After drying, we recover the dry OTS surface prior to contact before water and PDMS.

We complemented the SSP SFG spectra with SPS polarization to test for OTS ordering under different contacting conditions. SPS polarization results are sensitive to the orientation of the all-trans self-assembled OTS chains.[31,40] A single peak at 2950 cm^{-1} indicates a well-ordered film,[31] consistent with the order seen with SSP SFG results (Supporting Information, Figure S1a−c). We have also measured the SFG spectra in D_2O to avoid any confusion with the spectral interpretation of confined water and the surface OH peak of the sapphire substrate both dry and wet shown in Figure 3e. These results support the conclusion that the contact interface between PDMS−OTS underwater is dry. The SFG results are consistent with dry contact hypothesized from the JKR measurements and those calculated using the Young−Dupré equation. Additionally, the complete recovery of the interfacial structure was consistent with the small hysteresis observed for PDMS−OTS JKR measurements underwater.

It is interesting that the SFG results for PDMS−PVNODC surfaces in contact underwater (Figures 3c,d) are strikingly different from the PDMS−OTS contact. SFG observes structural rearrangements of PVNODC with the addition of water by a pronounced methylene symmetric peak at 2860 cm^{-1} and a methylene asymmetric peak at 2920 cm^{-1} (Figure 3g). The methyl symmetric peak at 2870−75 cm^{-1} and methyl Fermi peak at 2930 cm^{-1} are also observed in the SFG spectra, indicating that not all methyl chains are disordered upon contact with water. In contact with PDMS, the PVNODC interface shows very different spectral features compared to those in dry or wet contact. A restructured contact interface shows peak assignments at 2850, 2875, and 2935 cm^{-1}, representing a shifted $CH_{2,sym}$, $CH_{3,sym}$, and $CH_{3,Fermi}$.[31] There is also a peak at 2900−2905 cm^{-1}, possibly from Si−CH_3 from the contacting PDMS.[32] After separating the PDMS−PVNODC contact, the spectral features are almost recovered. The small differences before and after contact are in the relative intensities of the methyl and methylene peaks. After drying, the PVNODC air surface is the same as observed prior to water and PDMS contact.

DOI: 10.1021/la504564w
Langmuir 2015, 31, 2398−2406

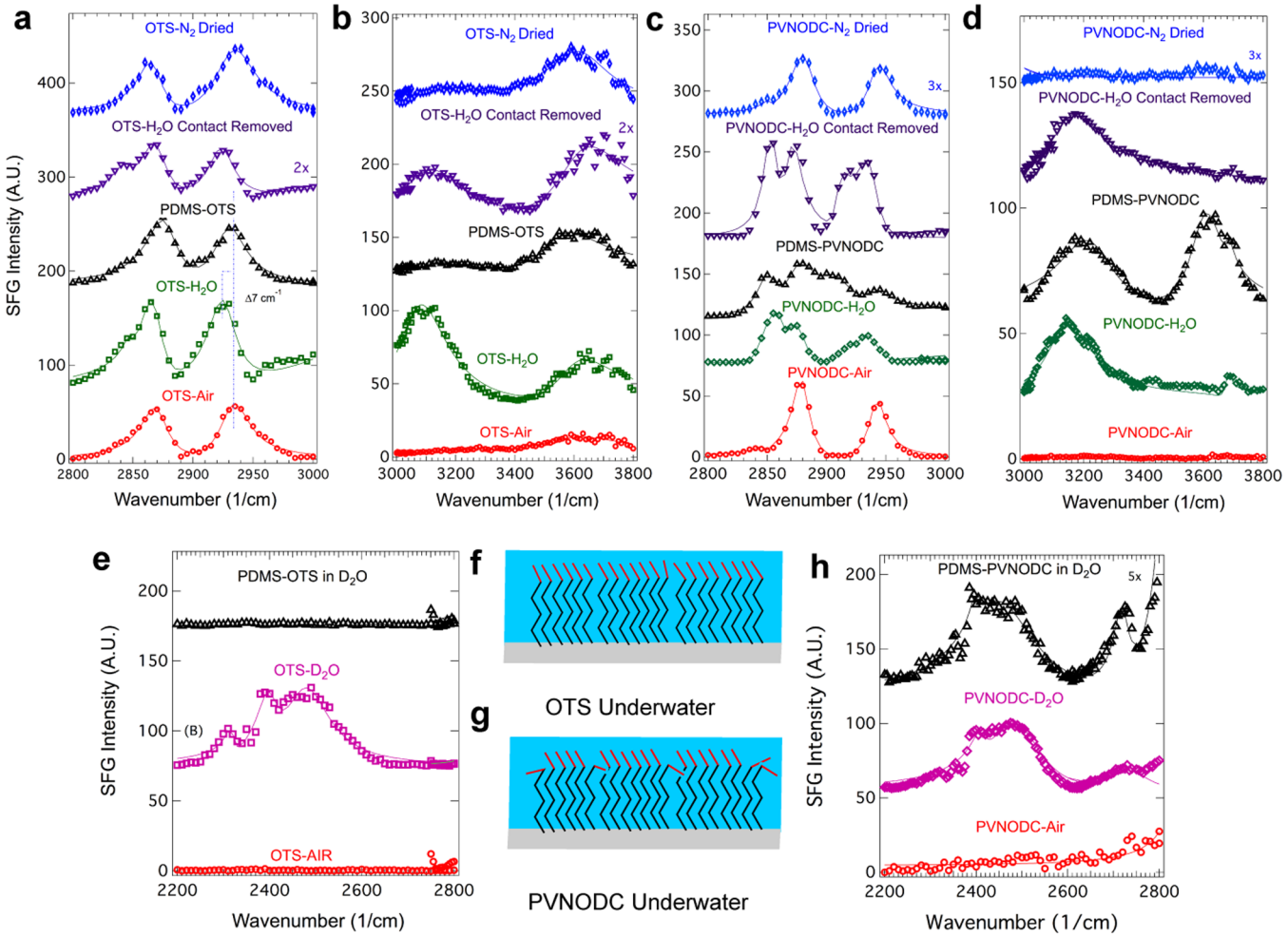

Figure 3. SFG spectroscopy of wet mechanical contact of elastomeric PDMS on OTS and PVNODC probed by SFG. The spectra are shown in the hydrocarbon region (2800−3000 cm^{-1}) and water region (3000−3800 cm^{-1}) in SSP polarization and separated for clarity for different measured interfaces during the experiment: air, water, underwater contact, removed underwater contact, and dried for (a) PDMS−OTS hydrocarbon region, (b) PDMS−OTS water region, (c) PDMS−PVNODC hydrocarbon region, and (d) PDMS−PVNODC water region. Spectra in the D_2O region (2200−2800 cm^{-1}) for mechanical contact of PDMS with (e) OTS (PPP polarization) and (h) PVNODC (SSP polarization) in the presence of D_2O. Sketch of (f) OTS and (g) PVNODC surface structure at the water interface.

The spectra in the water region offer some interesting insight into the nature of the contact interface. The PVNODC surface in contact with water shows a small peak near 3700 cm^{-1}, indicating interactions of OH groups of water with hydrophobic groups (van der Waals interactions). This has been observed for water in contact with OTS surfaces.[41] It is also possible that the signal in the 3700 cm^{-1} region could be due to surface OH from the sapphire substrate, as seen with OTS (Supporting Information, Figure S1b). However, we have ruled this hypothesis out due to several reasons. First, we have spin-coated PVNODC films with thicknesses of ≈300 nm to minimize the contributions from the sapphire substrate. The predictions of the SFG intensity in SSP polarization as a function of film thickness are provided in the Supporting Information (Figures S3a−d). Second, no such peak is observed for PVNODC in contact with D_2O (Figure S3b) in the H_2O region. Instead, we observed a strong hydrogen-bonded OD peak at 2410 cm^{-1} and a second OD peak near 2725−30 cm^{-1} (associated with OD in contact with hydrophobic methyl groups).

The spectra for PVNODC in contact with PDMS underwater show that a strongly hydrogen-bonded water peak (3225 cm^{-1}) was still present, indicating that the water was not squeezed out from the contact region. Because PVNODC is semicrystalline, it is unlikely that water has penetrated or absorbed into the film. We observed a second peak in the water region near 3600−3650 cm^{-1}, associated with the OH groups of water interacting with PDMS or PVNODC.[42] This peak is shifted with respect to that observed due to van der Waals interactions of OH group in contact with hydrophobic groups (3700 cm^{-1}). We have again verified that the peak near 3605 cm^{-1} is not due to the contribution from surface OH groups at the PVNODC−sapphire interface. When H_2O is replaced with D_2O, we observed no peaks in the H_2O region (3200−3800 cm^{-1}), and spectral peaks were observed in the D_2O region (2300−2800 cm^{-1}) for PVNODC in contact with PDMS. A strongly hydrogen-bonded OD peak was observed at 2395 cm^{-1} and a second peak at 2720 cm^{-1}. This second peak is not as shifted as what we observed for confined water. An increase in the signal intensity and narrowing of line width suggests an increase in ordering of the confined water between the two surfaces. After separating the PDMS−PVNODC contact, the spectral features in the water region were reversible. The differences in the spectral signatures before and after contact

DOI: 10.1021/la504564w
Langmuir 2015, 31, 2398−2406

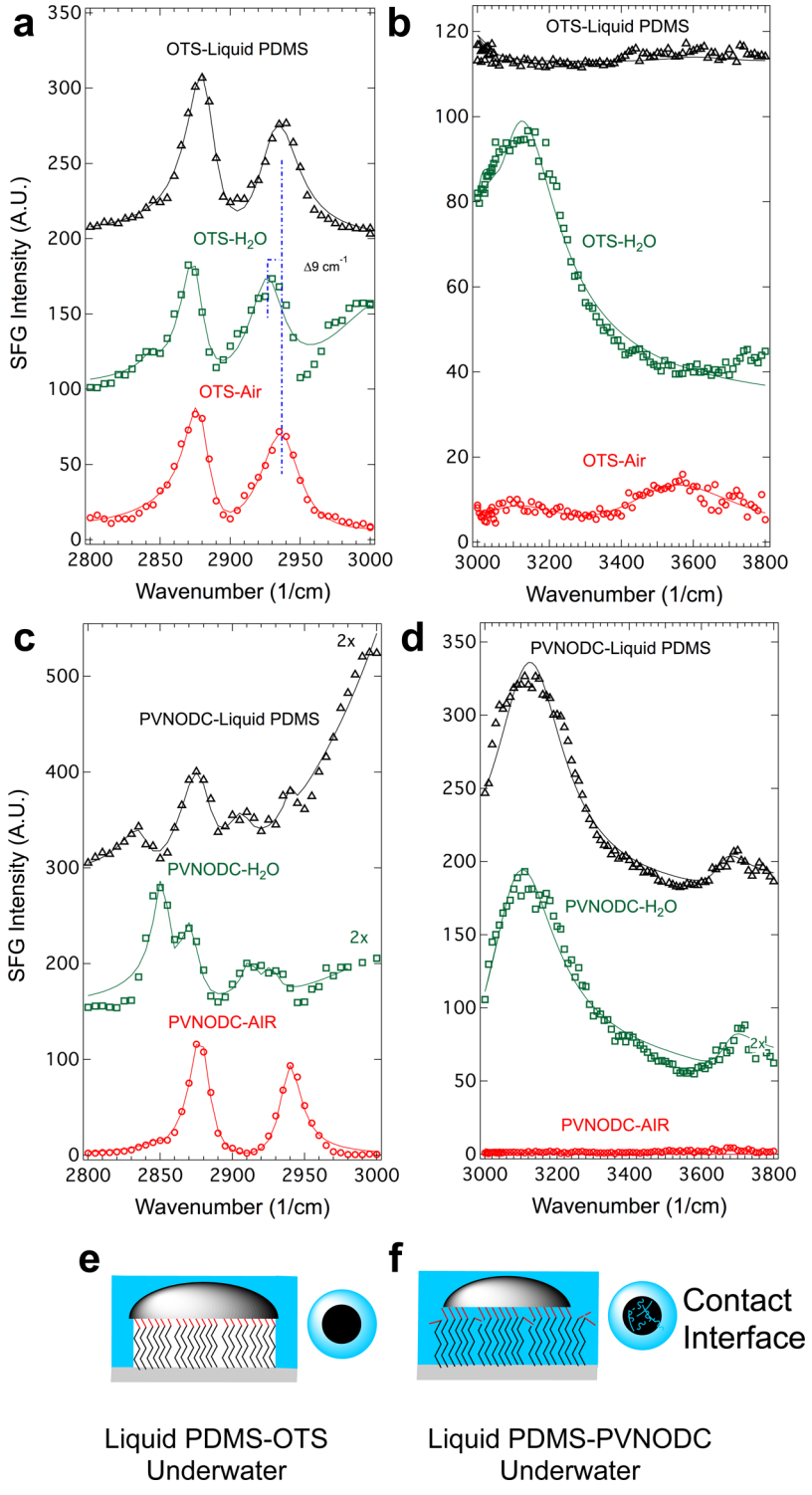

Figure 4. SFG spectroscopy wet contact of liquid PDMS on OTS and PVNODC. The spectra are shown in the hydrocarbon region (2800−3000 cm^{-1}) and water region (3000−3800 cm^{-1}) in SSP polarization and separated for clarity for different measured interfaces during the experiment: air, water, underwater for (a) liquid PDMS−OTS hydrocarbon region, (b) liquid PDMS−OTS water region, (c) liquid PDMS−PVNODC hydrocarbon region, and (d) liquid PDMS−OTS water region. The adhesion energy and low elasticity prevent the removal of the contacting drop underwater. Sketch, profile and top view, of the contact made of liquid PDMS on (e) OTS and (f) PVNODC underwater.

also explain the higher adhesion hysteresis observed for PDMS−PVNODC compared to the PDMS−OTS contact interfaces. The lowered W_a underwater was a result of the decrease in PVNODC−H_2O interfacial energy caused by molecular rearrangements and the presence of confined water observed by SFG.

We ruled out the differences in adhesion values for PDMS in contact with OTS and PVNODC underwater due to differences in surface roughness[43,44] because the surface energies obtained from the dry JKR measurements are consistent for smooth surfaces. In addition, the surface roughness of dry PVNODC was measured to be rms = 0.3 nm by atomic force microscopy,

DOI: 10.1021/la504564w
Langmuir 2015, 31, 2398−2406

similar to the roughness of an OTS-coated sapphire substrate.[31] We do not expect the roughness of PVNODC to change drastically underwater because we are below the melting point[31] of PVNODC.

By our estimates, the trapping of macroscopic interfacial water is not due to the hydrodynamic forces required to drain water. The drainage force, $F_{drainage} = 6\pi\eta v r^2/h$, from a 20 nm thin film is less than the force applied (20 nN (drainage) < 10 mN (applied)) and should decrease with time. From Reynold's theory, the drainage time $h \sim t^{-0.5}$ is predicted as $t_{drainage} < 3$ ms[45] (SI7). Both JKR and SFG experiments were slower than the calculated water drainage between two rigid surfaces($t_{exp,JKR} \sim 3-5$ s, $t_{exp,SFG} \sim 20$ min). In addition, we do not expect $t_{drainage}$ to be dramatically different for OTS and PVNODC surfaces. It is more likely that the rearrangement of PVNODC hydrophobic side chains at the grain boundary may be responsible for the interstitial water, resulting in the lowered W_a.[31] However, the differences in adhesion energy between the JKR and calculated by the Young–Dupré results are still not understood.

We hypothesized that liquid PDMS contact with OTS or PVNODC results in dry contact, and we tested this by probing the molecular structure of these contact interfaces (Figure 4a–d). For the liquid PDMS–OTS, we observed the same spectral features that we observed for a cross-linked PDMS lens in contact with an OTS surface, indicating that the contact is dry and that the structure of the OTS was similar to that observed in contact with air (Figure 4e). This confirmed our hypothesis of dry contact underwater from JKR and Young–Dupré measurements.

Similar experiments with liquid PDMS in contact with PVNODC underwater resulted in surprising results. We observed the same spectral features in the hydrocarbon region for liquid PDMS and cross-linked PDMS, with a slight change in the relative intensities of the methylene asymmetric peak at 2915 cm^{-1} and methyl Fermi peak at 2930 cm^{-1} (Figures 4c,d). In the water region, we observed a strongly hydrogen-bonded water peak (3115 cm^{-1}) and a peak associated with OH groups in contact with hydrophobic surfaces (3700 cm^{-1}). The strongly hydrogen-bonded water peak was similar to that of confined water between PDMS lens and PVNODC substrate. However, there were differences in the peak position of the second OH peak at higher wavenumbers. This suggests that there are some structural differences between the confined water between liquid PDMS and PDMS elastomer. In addition, the spectroscopy shows that the liquid PDMS in contact with PVNODC is not a dry contact as indicated by the results of the W_a calculated using the Young–Dupré equation. Interestingly, the presence of confined interstitial water has a huge impact on the W_a measured using contact mechanics, yet no influence on the W_a calculated using the Young–Dupré equation.

The key to understanding the discrepancy in the W_a measured by JKR and calculated by the Young–Dupré equation is the observation of heterogeneous contact between PDMS and the PVNODC surface underwater (Figure 4f). If the contact was homogeneous, then the Young–Dupré equation should have predicted the same W_a measured using JKR. If the region near the contact line is dry (no confined water), then the Young–Dupré equation will not be sensitive to the confined water in the interior regions, and this would result in the failure of the Young–Dupré equation in predicting the adhesive energy. Stated differently, for heterogeneous surfaces, the Young–Dupré equation would be valid only if the heterogeneity is represented in the contact line.[33] Simulations have found the role of heterogeneity on adhesion at an atomistic length scale,[23] but our findings experimentally confirm what others have theorized at a molecular length scale. In addition, it was only possible to demonstrate the failure of the Young–Dupré equation by combining measurements of dry and wet adhesion, wetting, and *in situ* SFG spectroscopy at the contact interface underwater.

Finally, we derived a Young–Dupré equation to calculate the fraction of the total area occupied by water (f_w) using the measured angle of liquid PDMS on PVNODC ($\theta_{PDMS,PVNODC}$) underwater.

$$W_a = (1 - f_w)(\gamma_{PDMS,H_2O})(1 + \cos(\theta_{PDMS,PVNODC})) \quad (3)$$

This equation predicts that the heterogeneous W_a will be lower by a factor of $(1 - f_w)$ compared to homogeneous contact. Using the measured $W_{a,JKR} = 45$ mJ/m^2, $\gamma_{PDMS,H_2O} = 41$ mJ/m^2, and contact angle measured by placing a drop of liquid PDMS in contact with PVNODC substrate underwater (30°), we predict $f_w = 0.41$. The defects in the ordered layer of hydrophobic PVNODC side chains at the crystalline grain boundaries in contact with water have a profound effect in sequestering water at the PDMS–PVNODC interface underwater.

CONCLUSIONS

The presence of interstitial water results from subtle hydrophobic surface rearrangements of the PVNODC interface and has profound importance in many fields with systems far greater in complexity. For example, the removal of water molecules is necessary for protein hydrophobic collapse[3] or the function of the lock and key model prevalent in enzyme catalysis.[22] Interstitial water also has implications for kinetics in dewetting models[44] or how animals achieve strong underwater contact.[46,47] Overall, this work raises questions about the salient features that promote or prohibit the removal of water between interfaces,[19] the impact of heterogeneity on interfacial processes,[23] and the need to further develop models for hydrophobic interactions.[5] Finally, the presence of interstitial water leads to the breakdown of the Young–Dupré equation that has been used extensively in the literature and highlights the direct need to understand the contacting interface.

ASSOCIATED CONTENT

Supporting Information

Details on adhesion theory from JKR and contact angle measurements and further information on material preparation and instrumentation measurement details; supporting SFG spectroscopy referenced in the main text. This material is available free of charge via the Internet at http://pubs.acs.org.

AUTHOR INFORMATION

Corresponding Author

*E-mail: ali4@uakron.edu (A.D.).

Notes

The authors declare no competing financial interest.

ACKNOWLEDGMENTS

The authors thank Mr. Ed McLaughlin for construction and fabrication of instrumental devices and Ms. Nasim Rhamani (Kansas State University) and Dr. Bi-Min Newby (University of Akron) for useful discussions on underwater JKR measure-

DOI: 10.1021/la504564w
Langmuir 2015, 31, 2398–2406

ments. In addition, we thank Mr. Gaurav Amarpuri, Mr. He Zhu, Mrs. Dona Foster, Mrs. Diane Gorse, Ms. Saranshu Singla, and Ms. Mena Klittich for discussions. We thank the financial support of National Science Foundation (AD) and the Akron Functional Materials Center (MLB).

REFERENCES

(1) Kauzmann, W. Some Factors in the Interpretation of Protein Denaturation. *Adv. Protein Chem.* **1959**, *14*, 1−63.
(2) Baldwin, R. L. Temperature Dependence of the Hydrophobic Interaction in Protein Folding. *Proc. Natl. Acad. Sci. U. S. A.* **1986**, *83*, 8069−8072.
(3) Zhou, R. Hydrophobic Collapse in Multidomain Protein Folding. *Science* **2004**, *305*, 1605−1609.
(4) Whitesides, G.; Mathias, J. P.; Seto, C. T. Molecular Self-Assembly and Nanochemistry: A Chemical Strategy for the Synthesis of Nanostructures. *Science* **1991**, *254*, 1312−1319.
(5) Chandler, D. Interfaces and the Driving Force of Hydrophobic Assembly. *Nature* **2005**, *437*, 640−647.
(6) Huang, X.; Margulis, C. J.; Berne, B. J. Dewetting-Induced Collapse of Hydrophobic Particles. *Proc. Natl. Acad. Sci. U. S. A.* **2003**, *100*, 11953−11958.
(7) Berne, B. J.; Weeks, J. D.; Zhou, R. Dewetting and Hydrophobic Interaction in Physical and Biological Systems. *Annu. Rev. Phys. Chem.* **2009**, *60*, 85−103.
(8) Kurutz, J. W.; Xu, S. Hofmeister Solute Effects on Hydrophobic Adhesion Forces in SFM Experiments. *Langmuir* **2001**, *17*, 7323−7326.
(9) Min, T.; Kim, J. Effects of Hydrophobic Surface on Skin-Friction Drag. *Phys. Fluids* **2004**, *16*, L55.
(10) Mrksich, M.; Whitesides, G. Using Self-Assembled Monolayers to Understand the Interactions of Man-Made Surfaces with Proteins and Cells. *Annu. Rev. Biophys. Biomol. Struct.* **1996**, *25*, 55−78.
(11) Marrink, S.-J.; Berendsen, H. J. Simulation of Water Transport through a Lipid Membrane. *J. Phys. Chem.* **1994**, *98*, 4155−4168.
(12) Vinogradova, O. I. Drainage of a Thin Liquid Film Confined between Hydrophobic Surfaces. *Langmuir* **1995**, *11*, 2213−2220.
(13) Breslow, R. Hydrophobic Effects on Simple rganic Reactions in Water. *Acc. Chem. Res.* **1991**, *24*, 159−164.
(14) Israelachvili, J. N. *Intermolecular and Surface Forces*, 2nd ed.; Academic Press: San Diego, CA, 1991.
(15) Pashley, R.; McGuiggan, P.; Ninham, B.; Evans, D. Attractive Forces Between Uncharged Hydrophobic Surfaces: Direct Measurements in Aqueous Solution. *Science* **1985**, *229*, 1088−1089.
(16) Rabinovich, Y. I.; Yoon, R.-H. Use of Atomic Force Microscope for the Measurements of Hydrophobic Forces Between Silanated Silica Plate and Glass Sphere. *Langmuir* **1994**, *10*, 1903−1909.
(17) Christenson, H. K.; Claesson, P. M. Cavitation and the Interaction Between Macroscopic Hydrophobic Surfaces. *Science* **1988**, *239*, 390−392.
(18) Clint, J. H.; Wicks, A. C. Adhesion under Water: Surface Energy Considerations. *Int. J. Adhes. Adhes.* **2001**, *21*, 267−273.
(19) Lei, Y.; Leng, Y. Hydrophobic Drying and Hysteresis at Different Length Scales by Molecular Dynamics Simulations. *Langmuir* **2012**, *28*, 3152−3158.
(20) Koishi, T.; Yasuoka, K.; Ebisuzaki, T.; Yzfoo, S.; Zeng, X. C. Large-Scale Molecular-Dynamics Simulation of Nanoscale Hydrophobic Interaction and Nanobubble Formation. *J. Chem. Phys.* **2005**, *123*, 204707.
(21) Yu, B.; Blaber, M.; Gronenborn, A. M.; Clore, G. M.; Caspar, D. Disordered Water within a Hydrophobic Protein Cavity Visualized by X-ray Crystallography. *Proc. Natl. Acad. Sci. U. S. A.* **1999**, *96*, 103−108.
(22) Snyder, P. W.; Mecinović, J.; Moustakas, D. T.; Thomas, S. W.; Harder, M.; Mack, E. T.; Lockett, M. R.; Héroux, A.; Sherman, W.; Whitesides, G. M. Mechanism of the Hydrophobic Effect in the Biomolecular Recognition of Arylsulfonamides by Carbonic Anhydrase. *Proc. Natl. Acad. Sci. U. S. A.* **2011**, *108*, 17889−17894.
(23) Giovambattista, N.; Debenedetti, P. G.; Rossky, P. J. Hydration Behavior under Confinement by Nanoscale Surfaces with Patterned Hydrophobicity and Hydrophilicity. *J. Phys. Chem. C* **2007**, *111*, 1323−1332.
(24) Ocko, B.; Dhinojwala, A.; Daillant, J. Comment on How Water Meets a "Hydrophobic Surface. *Phys. Rev. Lett.* **2008**, *101*, 039601.
(25) Mezger, M.; Reichert, H.; Schöder, S.; Okasinski, J.; Schröder, H.; Dosch, H.; Palms, D.; Ralston, J.; Honkimäki, V. High-Resolution in Situ X-ray Study of the Hydrophobic Gap at the Water-Octadecyl-Trichlorosilane Interface. *Proc. Natl. Acad. Sci. U. S. A.* **2006**, *103*, 18401−18404.
(26) Parker, J. L.; Claesson, P. M.; Attard, P. Bubbles, Cavities, and the Long-Ranged Attraction between Hydrophobic Surfaces. *J. Phys. Chem.* **1994**, *98*, 8468−8480.
(27) Jamadagni, S. N.; Godawat, R.; Garde, S. Hydrophobicity of Proteins and Interfaces: Insights from Density Fluctuations. *Annu. Rev. Chem. Biomol. Eng.* **2011**, *2*, 147−171.
(28) Kinning, D. J. Surface and Interfacial Structure of Release Coatings for Pressure Sensitive Adhesives I. Polyvinyl N-Alkyl Carbamates. *J. Adhes.* **1997**, *60*, 249−274.
(29) Chaudhury, M. K.; Whitesides, G. M. Direct Measurement of Interfacial Interactions between Semispherical Lenses and Flat Sheets of Poly(dimethylsiloxane)and Their Chemical Derivatives. *Langmuir* **1991**, *7*, 1013−1025.
(30) Loskofsky, C.; Song, F.; Newby, B.-m. Z. Underwater Adhesion Measurements using the JKR Technique. *J. Adhes.* **2006**, *82*, 713−730.
(31) Rangwalla, H.; Schwab, A. D.; Yurdumakan, B.; Yablon, D. G.; Yeganeh, M. S.; Dhinojwala, A. Molecular Structure of an Alkyl-Side-Chain Polymer-Water Interface: Origins of Contact Angle Hysteresis. *Langmuir* **2004**, *20*, 8625−8633.
(32) Yurdumakan, B.; Nanjundiah, K.; Dhinojwala, A. Origin of Higher Friction for Elastomers Sliding on Glassy Polymers. *J. Phys. Chem. C* **2007**, *111*, 960−965.
(33) Gao, L.; McCarthy, T. J. How Wenzel and Cassie Were Wrong. *Langmuir* **2007**, *23*, 3762−3765.
(34) Lambert, A. G.; Davies, P. B.; Neivandt, D. J. Implementing the Theory of Sum Frequency Generation Vibrational Spectroscopy: A Tutorial Review. *Appl. Spectrosc. Rev.* **2005**, *40*, 103−145.
(35) Li, G.; Dhinojwala, A.; Yeganeh, M. S. Interference Effect from Buried Interfaces Investigated by Angular-Dependent Infrared-Visible Sum Frequency Generation Technique. *J. Phys. Chem. C* **2011**, *115*, 7554−7561.
(36) Harp, G. P.; Dhinojwala, A. Direct Probe of Interfacial Structure during Mechanical Contact between Two Polymer Films Using Infrared Visible Sum Frequency Generation Spectroscopy. *J. Adhes.* **2005**, *81*, 371−379.
(37) Choi, G. Y.; Kim, S.; Ulman, A. Adhesion Hysteresis Studies of Extracted Poly(dimethylsiloxane) Using Contact Mechanics. *Langmuir* **1997**, *13*, 6333−6338.
(38) Li, L.-H.; Macosko, C.; Korba, G. L.; Pocius, A. V.; Tirrell, M. Interfacial Energy and Adhesion between Acrylic Pressure Sensitive Adhesives and Release Coatings. *J. Adhes.* **2001**, *77*, 95−123.
(39) Yurdumakan, B.; Harp, G. P.; Tsige, M.; Dhinojwala, A. Template-Induced Enhanced Ordering under Confinement. *Langmuir* **2005**, *21*, 10316−10319.
(40) Tyrode, E.; Liljeblad, J. F. D. Water Structure Next to Ordered and Disordered Hydrophobic Silane Monolayers: A Vibrational Sum Frequency Spectroscopy Study. *J. Phys. Chem. C* **2013**, *117*, 1780−1790.
(41) Tian, C. S.; Shen, Y. R. Structure and Charging of Hydrophobic Material/Water Interfaces Studied by Phase-Sensitive Sum-Frequency Vibrational Spectroscopy. *Proc. Natl. Acad. Sci. U. S. A.* **2009**, *106*, 15148−15153.
(42) Kurian, A.; Prasad, S.; Dhinojwala, A. Direct Measurement of Acid-Base Interaction Energy at Solid Interfaces. *Langmuir* **2010**, *26*, 17804−17807.
(43) Fuller, K.; Tabor, D. The Effect of Surface Roughness On the Adhesion of Elastic Solids. *Proc. R. Soc. London, Ser. A* **1975**, *345*, 327−342.

DOI: 10.1021/la504564w
Langmuir 2015, 31, 2398−2406

(44) Persson, B.; Volokitin, A. I.; Tosatti, E. Role of the External Pressure on the Dewetting of Soft Interfaces. *Eur. Phys. J. E: Soft Matter Biol. Phys.* **2003**, *11*, 409−413.
(45) Martin, P.; Brochard-Wyart, F. Dewetting at Soft Interfaces. *Phys. Rev. Lett.* **1998**, *80*, 3296.
(46) Stark, A. Y.; Badge, I.; Wucinich, N. A.; Sullivan, T. W.; Niewiarowski, P. H.; Dhinojwala, A. Surface Wettability Plays a Significant Role in Gecko Adhesion Underwater. *Proc. Natl. Acad. Sci. U. S. A.* **2013**, *110*, 6340−6345.
(47) Persson, B. N. J. Wet Adhesion with Application to Tree Frog Adhesive Toe Pads and Tires. *J. Phys.: Condens. Matter* **2007**, *19*, 376110.

DOI: 10.1021/la504564w
Langmuir 2015, 31, 2398−2406